Geophys. J. Int. (2002) **151,** 632–645

Crustal velocity model along the southern Cuban margin: implications for the tectonic regime at an active plate boundary

Bladimir Moreno,[1,2] Margaret Grandison[1,3] and Kuvvet Atakan[1]

[1] *Institute of Solid Earth Physics, University of Bergen, Allégaten* 41, 5007 *Bergen, Norway. E-mail: bladimir@ifjf.uib.no*
[2] *Centro Nacional de Investigaciones Sismológicas, CENAIS,* Calle 17 No 61 e/4 y 6, *Vista Alegre, Santiago de Cuba, Cuba. E-mail: bladimir@sssn.ciges.inf.cu*
[3] *Earthquake Unit, University of the West Indies, Mona Campus, Kingston* 7, *Jamaica*

Accepted 2002 June 26. Received 2002 April 9; in original form 2001 September 4

SUMMARY

A new 1-D velocity model along the southern Cuban margin has been determined using local earthquake data, which are the result of the merged Cuban and Jamaican catalogues. Simultaneous inversion using joint-hypocentre determination was applied to solve the coupled hypocentre–velocity model problem. We obtained a seven-layer model with an average Moho interface at 20 km. The average velocity was found to be 7.6 km s^{-1} on the top of the crust–mantle transition zone and 6.9 km s^{-1} in the basaltic layer of the crust. The improvement in the earthquake locations allowed us for the first time to use local seismicity to characterize the activity on local faults and the stress regime in the area. For this purpose, 34 earthquake focal mechanisms were determined along the eastern segments of the Oriente Fault. These solutions are consistent with the known left-lateral strike-slip motion along this major structure as well as with the stress regime of two local structures: (1) the Cabo Cruz Basin and (2) the Santiago deformed belt. The first structure is dominated by normal faults with minor strike-slip components and the second by reverse faults. The shallow seismicity in the Cabo Cruz Basin is associated with fault planes trending N55°–58°E and dipping 38°–45° to the north. The Santiago deformed belt, on the other hand, exhibits diverse fault plane orientations. These local structures account for most of the earthquake activity along the southern Cuban margin. Deep seismicity observed in the Santiago deformed belt, supported by focal mechanisms, suggests underthrusting of the Gonave Microplate beneath the Cuban Block in this area. The principal stress orientations obtained from stress inversion of earthquake focal mechanisms suggest a thrust faulting regime along the Southern Cuban margin. We obtained a nearly horizontal σ_1 and nearly vertical σ_3, which indicates active compressional deformation along the major Oriente transcurrent fault in agreement with the dominant structural trend associated with the Santiago deformed belt.

Key words: crustal structure, Cuba, focal mechanisms, seismicity, stress, tectonic, velocity model.

1 INTRODUCTION

The Oriente Fault (OF) presents the highest seismic hazard in the southern Cuban margin. It defines a segment of the North American and the Caribbean Plate boundary along which strike-slip deformation dominates (Fig. 1). Much of this deformation is concentrated along the releasing and restraining bends of the OF such as the Cabo Cruz Basin (CCB) and the Santiago deformed belt (SDB). This zone, comprising part of the Bartlett–Cayman fault system, is responsible for more than 90 per cent of the seismicity and the largest earthquakes observed along the southern Cuban margin. According to historical data there have been 19 strong earthquakes during the last 400 years with intensity VII or higher on the MSK scale (Alvarez *et al.* 1973). Earthquakes of magnitude 7 have occurred in this zone. The most recent strong earthquake recorded in this area took place on 1992 May 25th with a magnitude (M_s) of 6.9 and with a hypocentre located in the CCB (Perrot *et al.* 1997). We define the term 'Oriente Fault Zone' (OFZ) to include all structural features in the area between 79.5° and 73.5°W longitude and 19° and 20°N latitude, such as the CCB and SDB (Fig. 1).

Previous studies of crustal structure conducted for this area (Ewing *et al.* 1960; Edgar *et al.* 1971; Goreau 1983; Calais & Mercier de Lépinay 1990, 1991; Case *et al.* 1990; Donnelly 1994) were mostly based on seismic refraction, reflection and gravity measurements. These studies have shown a complex crustal structure with very irregular crustal thicknesses and seismic *P*-wave

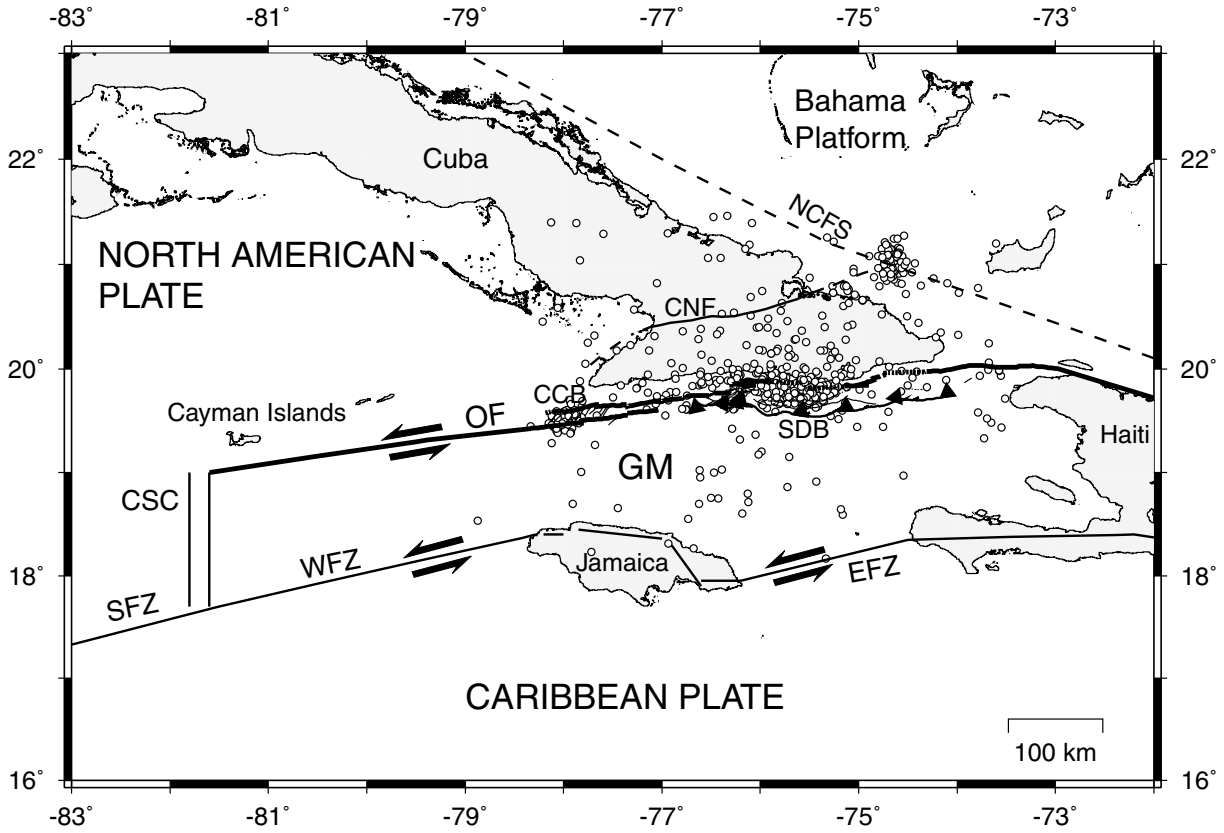

Figure 1. Kinematic framework along the southern Cuban margin. OF, Oriente fault; WFZ, Walton fault zone; EFZ, Enriquillo fault zone; CNF, Cauto Nipe fault; NCFS, Nortecubana fault system; SFZ, Swan fracture zone; CSC, Cayman spreading centre; GM, Gonave Microplate; CCB, Cabo Cruz Basin; SDB, Santiago deformed belt. The mapped OF including the CCB and SDB is taken from the interpretation made by Calais & Mercier de Lépinay (1990, 1991) during the SEACARIB II oceanographic cruise. Dashed lines represent assumed traces of faults. Open circles shows 569 earthquakes recorded by three or more stations during 1998 March–2000 July.

velocities. This inhomogeneity, together with the unfavourable geometrical arrangement of the Cuban Seismograph Network (CSN) (Fig. 2), makes it difficult to establish an average *P*-wave velocity model for the determination of the hypocentres. The Jamaican Seismic Network (JSN) (Fig. 2), the second local network recording data from this zone, is also located outside the OFZ. Owing to this uncertainty in earthquake locations, tectonic interpretation using local seismicity based on either of these networks alone has been difficult. In the present study, the earthquake data from the Cuban and the Jamaican seismic networks were merged to improve the location accuracy of earthquakes generated in the OFZ. The first objective of this work was to establish a reliable crustal velocity model. The obtained velocity model is then used for relocating the earthquakes with the aim of improved our understanding of the present tectonic regime in the area.

2 SOURCES OF DATA

The CSN is composes of six broad-band field stations along the island and five three-component telemetered short-period stations concentrated in the eastern part of Cuba. The JSN consists of 11 telemetered short-period stations, three of which have three components (Table 1 and Fig. 2). Both seismic networks are synchronized in time by the use of Global Positioning Systems (GPS). More information concerning the CSN and JSN can be found in Wiggins-Grandison (2001) and Moreno (2002).

A total of 99 earthquakes were collected from 1998 March to 2000 July (Fig. 2). Seven or more stations operating in both networks registered the seismic events, which had a local magnitude between 2.7 and 4.4. The criteria for selecting the data used in the inversion were for an earthquake to have 10 or more observed phases and an azimuthal gap of 180° and lower. This yielded only 60 earthquakes, so we included earthquakes with gaps up to 240°.

3 1-D VELOCITY MODEL

The part of the Caribbean Sea between Cuba and Jamaica has a complex crustal structure with lateral variations in seismic wave velocity and irregular thickness of oceanic crust. The crustal thickness varies between 5 and 20 km excluding water depth (Case *et al.* 1990). The Moho tends to be deeper along the south coast of Cuba and north coast of Jamaica. According to seismic refraction and reflection studies the *P*-wave velocity shows lateral variations from 7.8 to 8.2 km s^{-1} in the upper mantle and from 5.4 to 6.4 km s^{-1} in the basaltic layer of the crust (Ewing *et al.* 1960). Most of the Cuban seismic stations are located on a transitional crust, the interior part of the island arc with a range of crustal thicknesses from 17 to 30 km (Bush & Shcherbakova 1986). According to Bush & Shcherbakova (1986) the crust of Eastern Cuba can be divided into three layers: (1) a sedimentary volcanic layer with *P*-wave velocity from 4.0 to 4.8 km s^{-1}; (2) an upper layer of consolidated crust (5.8–6.4 km s^{-1}); and (3) a lower layer of consolidated crust

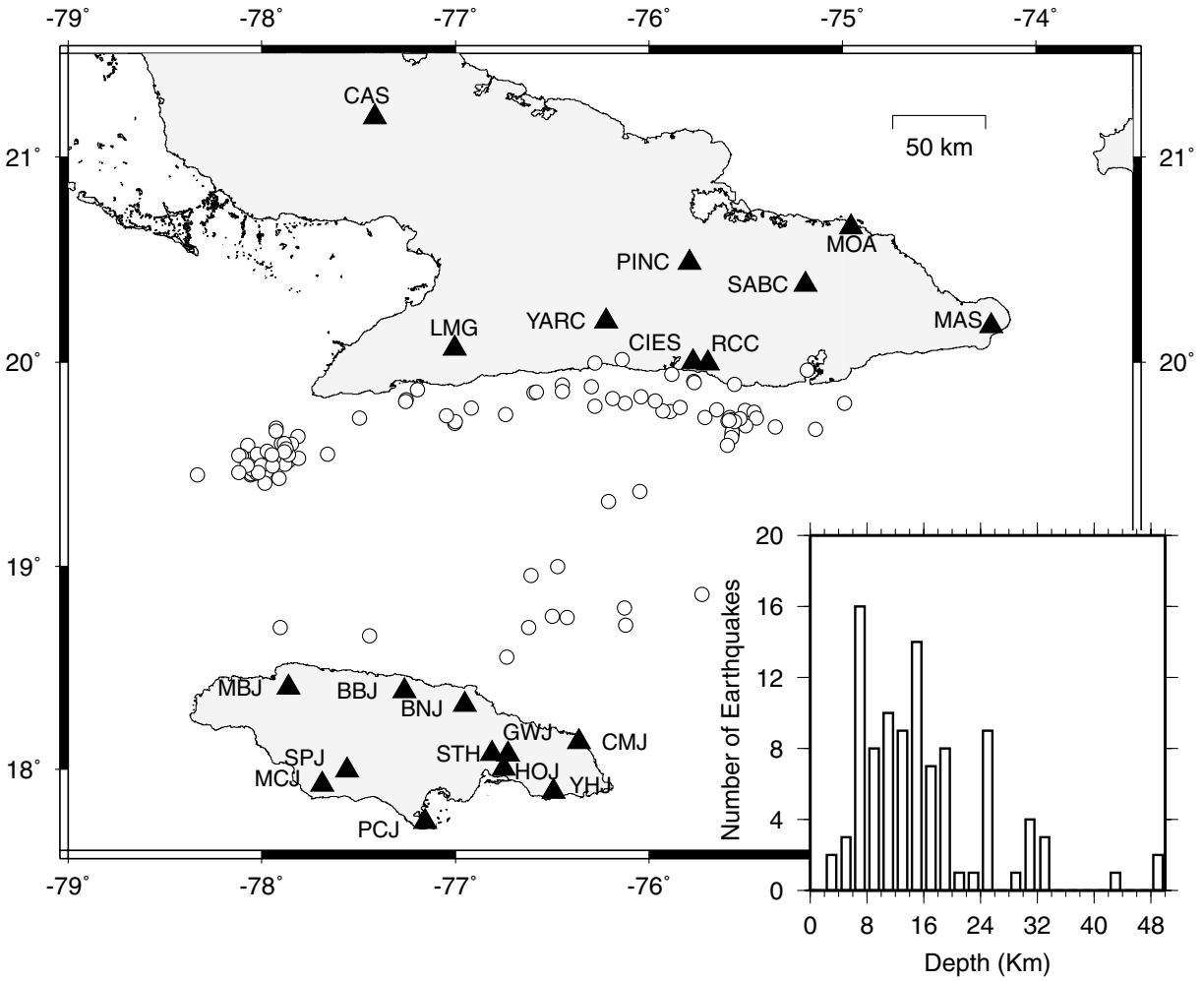

Figure 2. Seismic Networks of Cuba and Jamaica (black triangles) and epicentres of the earthquakes (open circles) used in the inversion process. The locations of the earthquakes were computed with the new velocity model obtained in this study. The inset shows the depth distribution of the earthquakes plotted in the map. The tick mark in the depth-axis assumes an interval of ±1 km.

(6.3–6.7 km s^{-1}). The Jamaican seismic stations are located on crust with an average thickness of 21 km. The basaltic crustal layer beneath the island is 12–15 km thick (Arden 1975).

3.1 Inversion process

The inversion process was achieved with the program VELEST (Kissling *et al.* 1995). The coupled hypocentre–velocity model problem was solved performing joint-hypocentre determination (JHD) using both *P* and *S* arrival times. The solution was obtained by a trial-and-error process with various initial velocity models and with different combinations of damping factors. For more details concerning the method see Kissling (1988) and Kissling *et al.* (1994).

No previous hypocentre–velocity structure inversion has been done for this area, therefore we used as the initial model for this inversion one of the available velocity models from the two networks involved (Fig. 3a). The Jamaican model was used to calculate the initial earthquake locations in the newly merged Cuban–Jamaican catalogue because more earthquakes had lower rms misfits when compared with the Cuban model (Fig. 5). The phase picks were reanalysed to reduce the number of badly picked phases. The number of observations per station of *P* and *S* waves is shown in Table 2.

The V_p/V_s ratio is an important parameter used by the inversion algorithm. To calculate this value we made a Wadati diagram using the SEISAN software (Havskov & Otemöller 1999) for the selected earthquakes and 1.74 was obtained with a standard deviation of 0.07. A reference station, which maintains its initial delay (normally set to zero) is also needed for the inversion process. Considering the spatial distribution of the earthquakes and the number of observations, we selected RCC as the control station (Fig. 2). This station has more than 85 per cent of the total readings and is located close to the major earthquake source.

The solution of the inverse problem depended strongly on the initial model and initial hypocentres. Since only 30 per cent of the selected earthquakes initially had an rms misfit below 0.5, we made several runs of VELEST using more earthquakes and a different initial model each time. After each run the velocity model obtained was used to relocate the entire catalogue and this served as the new input model for the next run. This procedure permitted us to increase the number of earthquakes having a low rms and then to use them as new initial hypocentres for the next run. Finally, we ended up with 89 earthquakes (90 per cent of the data) with an rms lower than or equal to 0.5 and a probable final model (Fig. 3a).

To test the variability of the convergence of the solution with respect to the input model, we ran VELEST with several input

Table 1. Seismic stations of Cuba and Jamaica used in this study with their delay time corrections.

Station	Instrument type and (no comp)	Latitude north (deg)	Longitude west (deg)	Elevation (m)	*P*-wave correction (s)	*S*-wave correction (s)
CCC	Broad B. (3)	21.1937	77.4172	90	1.22	3.37
RCC	Broad B. (3)	19.9953	75.6965	100	0.0	−0.15
LMG	Broad B. (3)	20.0673	77.0047	200	−0.02	0.08
CIES	Short P. (3)	20.0020	75.7710	40	−0.05	−0.10
YARC	Short P. (3)	20.2000	76.2200	100	−0.15	−0.10
PINC	Short P. (3)	20.4870	75.7910	647	0.00	0.96
SABC	Short P. (3)	20.3800	75.1900	100	−0.11	0.18
BBJ	Short P. (1)	18.3865	77.2623	766	−0.37	−1.14
BNJ	Short P. (1)	18.3210	76.9505	485	−0.43	−1.30
CMJ	Short P. (1)	18.1350	76.3613	333	−0.62	−1.02
GWJ	Short P. (1)	18.0742	76.7280	1170	−0.80	−1.35
HOJ	Short P. (1)	18.0050	76.7490	228	−0.41	−0.93
MBJ	Short P. (3)	18.4048	77.8630	513	−0.44	−1.07
MCJ	Short P. (3)	17.9253	77.6863	661	0.11	−0.19
PCJ	Short P. (1)	17.7412	77.1573	198	0.03	−0.45
SPJ	Short P. (1)	17.9960	77.5600	751	−0.40	−0.63
STH	Short P. (3)	18.0772	76.8097	504	−0.72	−1.19
YHJ	Short P. (1)	17.8920	76.4930	600	−0.29	−0.81
MOA	Broad B. (3)	20.6583	74.9568	140	−0.11	–
MAS	Broad B. (3)	20.1760	74.2310	350	0.83	–

models having different layer thickness and velocities (Fig. 3b). The input models do not have layer interfaces beyond 34 km owing to the shallow seismicity of the area and the known thickness of the crust. The set of solutions shows a similar geometry but indicates a large variability in the velocity range for the upper layers (Fig. 3c). The topmost layers did not converge very well owing to the small number of earthquakes with depths less than 7 km (inset of Fig. 2); most of the earthquakes are generated at more than 5 km below the seafloor. The rays arriving from bottom layers subvertically penetrate the topmost layers, therefore the ray lengths are shorter in the topmost layers and consequently, the traveltime segments carry less weight in the inversion process. The thinness and poor resolution of the topmost layers made the convergence of the inversion more difficult. Bottom layers show a tendency to converge within a very small velocity range. These results indicate that the inversion problem has a solution space with several local minima. How well the solution converges toward a local minimum depends on the initial model and the initial hypocentres.

The input models and their corresponding solutions indicate an average Moho depth of 20 km with velocities ranging between 7.5 and 7.7 km s^{-1}. The layer above the Moho up to 9 km depth exhibits a velocity range of 6.8–7.0 km s^{-1}. From the three probable solutions the one obtained using the input model with intermediate velocity had the lowest rms misfit. However, it is still not possible to claim that the absolute minimum of the solution space was found.

3.2 Selecting final model

The geometry of the final model was well defined by the inversion process. Selecting the velocity for each layer required an extra procedure. The range of velocities obtained from the simultaneous inversion for the near-surface layer was wide, so we used forward modelling to obtain a suitable solution. Several velocity models were tested using the HYPOCENTER program (Lienert & Havskov 1995) and the model with the overall lowest rms misfit was selected. According to the result of the inversion process and previous studies of seismic refraction, we defined a range of velocities for each layer to be tested. The input models consisted of eight layers with fixed thickness and wide variations in velocity. Table 3 shows the range of velocities for each layer to be tested with a velocity step of 0.1 km s^{-1}.

More than 1462 models were tested with the same set of data used for the inversion process. The final calculation ended with only one minimum corresponding to the input model shown in Table 4. This model is similar to the probable final model obtained in the previously described inversion process, but with more near-surface layers (Fig. 3d).

3.3 Station corrections

The delay times for each station (station corrections) are determined with the hypocentres and velocity model during the inversion process. Since we selected the final model using forward modelling, the station corrections had to be calculated again. In order to obtain the station corrections for *P* and *S* waves, we ran VELEST in the JHD mode with the new final velocity model and the same set of data used previously. The velocity model was damped to keep it fixed during the inversion process. The *P*-wave correction for the reference station was kept constant at the initial value (zero) and for the *S* wave was free floating. The resulting values of the station corrections ranged from −0.80 to 1.22 s for *P* waves and from −1.35 to 3.37 s for *S* waves (Table 1 and Fig. 4). The station corrections are traveltime residuals with respect to the reference station and represent local anomalies in the velocity. In the case of Cuba, the station corrections are also affected by velocity anomalies along the ray path. The effect of the path is cancelled when the earthquakes are widely distributed in the area. However, the seismicity in Cuba is clustered in a few zones (Fig. 1). The local topography at Cuban seismic stations has little influence on the station corrections. The elevation above sea level and soil conditions are not significantly different. The biggest values in the station corrections are associated with differences in crustal thickness and seismic wave velocities throughout the area. The control station (RCC) is located where the Moho is 18–20 km deep, whereas some of the stations

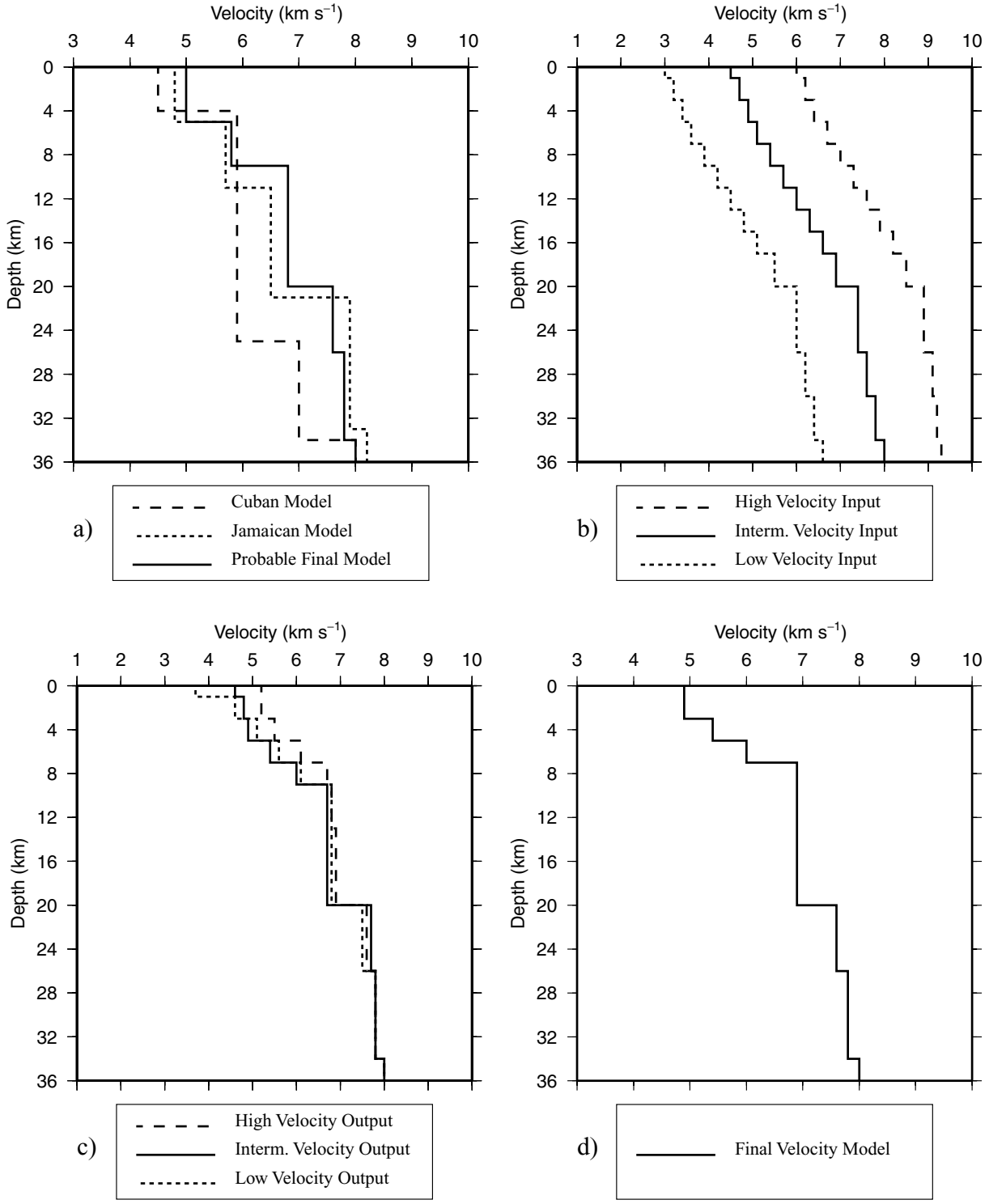

Figure 3. *P*-wave velocity models: (a) Cuban and Jamaican models and the probable final model derived from the inversion process; (b) input models used in the inversion process for testing the stability (convergence) of the solution proposed in (a); (c) output models of the inversion associated with the input models defined in (b); (d) final model obtained from forward modelling.

with high corrections values such as CAS are located where the Moho is 30 km deep (Bush & Shcherbakova 1986). The theoretical first arrival for this station should be a head-wave travelling along the Moho interface at 20 km depth, but in fact they have a longer ray path. The tendencies of negative values for the Jamaican stations are associated with first arrivals travelling southward at shallower Moho interfaces. The seismic rays coming from the major seismic sources are crossing a thin oceanic crust. Here, local topography and site conditions might also be affecting the station corrections.

Table 2. Number of observed phases for each station used in the inversion process.

Stations	No observ. of *P*	No observ. of *S*	Stations	No observ. of *P*	No observ. of *S*
STH	90	83	MCJ	20	14
RCC	85	65	PINC	23	8
GWJ	82	51	CMJ	19	11
LMG	77	68	CIES	15	10
BNJ	71	55	YHJ	11	11
CCC	62	41	SABC	10	7
BBJ	59	45	YARC	10	7
MBJ	52	50	MAS	8	–
PCJ	62	34	MOA	8	–
HOJ	36	29	SPJ	4	4

Table 3. Range of velocities to be tested in forward modelling using a step of 0.1 km s^{-1}.

Layer no	Velocity range (km s^{-1})	Depth (km)
1	4.3–4.9	0
2	4.9–5.4	3
3	5.4–6.0	5
4	6.0–6.9	7
5	6.9 (constant)	9
6	7.6 (constant)	20
7	7.8 (constant)	26
8	8.0 (constant)	34

Table 4. Final velocity model.

Layer no	Velocity (km s^{-1})	Depth (km)	Thickness (km)
1	4.9	0	3
2	5.4	3	2
3	6.0	5	2
4	6.9	7	13
5	7.6	20	6
6	7.8	26	8
Half-space	8.0	34	–

3.4 Relocation of the earthquakes

A total of 569 earthquakes recorded by three or more stations were collected during 2 years of monitoring (Fig. 1). The rms residuals in the hypocentre locations for the entire dataset computed with the obtained velocity model and the previous initial models are illustrated in Fig. 5. More than 55 per cent of the earthquakes have rms misfit lower than 0.5 s, which represents a significant improvement in the new earthquake locations when compared with the solutions obtained by using either the Cuban or Jamaican velocity models. The change in the earthquake locations using the new model with respect to the Cuban model is presented in Fig. 6. There are four boxes enclosing the zones with some tendencies in the orientation of the new location. Zone 'a' is associated with the seismicity of the CCB (Fig. 1). The new locations delineate this pull-apart zone very well. Zone 'b' moves the hypocentres southward in agreement with the location of the major Oriente strike-slip fault (Fig. 1). The new locations in zone 'c' move the hypocentres toward the SDB, and zone 'd' concentrates the aftershocks of the 1998 December 28th earthquake ($M_w = 5.6$) in the junction of the Cauto–Nipe fault (CNF) and the Nortecubana fault system (NCFS) (Fig. 1). The largest arrows are associated with the effect of changing an old solution with a very deep hypocentre to a new shallow solution. A summary of the location errors for the previous Cuban and Jamaican models and the new velocity model is given in Table 5.

4 THE TECTONIC REGIME OF THE AREA

The relative motion between the North American and Caribbean plates governs the tectonic regime of the area at a regional scale (Fig. 1). The eastward motion of the Caribbean plate relative to the North American plate has been debated to be at a rate from 12 to 40 mm yr^{-1} (Sykes *et al.* 1982; De Mets *et al.* 1990; Deng & Sykes 1995; Dixon *et al.* 1998). Most recently, De Mets *et al.* (2000) estimate an average of 18–20 $\pm$ 3 mm yr^{-1} with 18 $\pm$ 2 mm yr^{-1} of boundary parallel slip and 3 ± 3 mm yr^{-1} of boundary normal convergence south of eastern Cuba. This eastward motion of the Caribbean plate produces left-lateral slip along the Enriquillo (EFZ) and Walton Fault Zones (WFZ), and left-lateral strike-slip deformation along the OF (Fig. 1). However, there are two important local structures affecting the tectonic regime in the area: (1) the CCB and (2) the SDB (Fig. 1). These structures account for more than 90 per cent of the seismicity along this part of the plate boundary. Despite the fact that this area includes the best known and studied segment of the OFZ (Calais & Mercier de Lépinay 1991), small and moderate earthquakes have never been used as additional data to support the interpretations made in terms of the present tectonic regime. Fig. 1 also shows the aftershocks of a 5.6M_w earthquake that occurred on 1998 December 28th at the junction of the CNF and NCFS. The focal mechanism (from the Harvard CMT catalogue) gives almost pure reverse faulting along a direction parallel to the strike of the NCFS. We do not attempt any characterization of the tectonic regime in this area because of the poor station coverage. In this study, our focus is toward those structures located along the OFZ (the CCB and SDB).

4.1 Earthquake focal mechanisms and seismicity of the CCB and SDB

In order to correlate earthquake activity with active faults we solved for 34 earthquake focal mechanisms along the OFZ (Figs 7 and 8). Normally, the reliability of a focal mechanism solution depends on the size of the earthquake and the method used for the solution (e.g. moment tensor, waveform modelling, first motion) but in our case all the earthquakes are small ($M < 4.5$) and the focal mechanisms were determined by using only *P*-wave first-motion polarities. The solutions were obtained using the SEISAN software (Havskov & Otemöller 1999), which uses the algorithm developed by

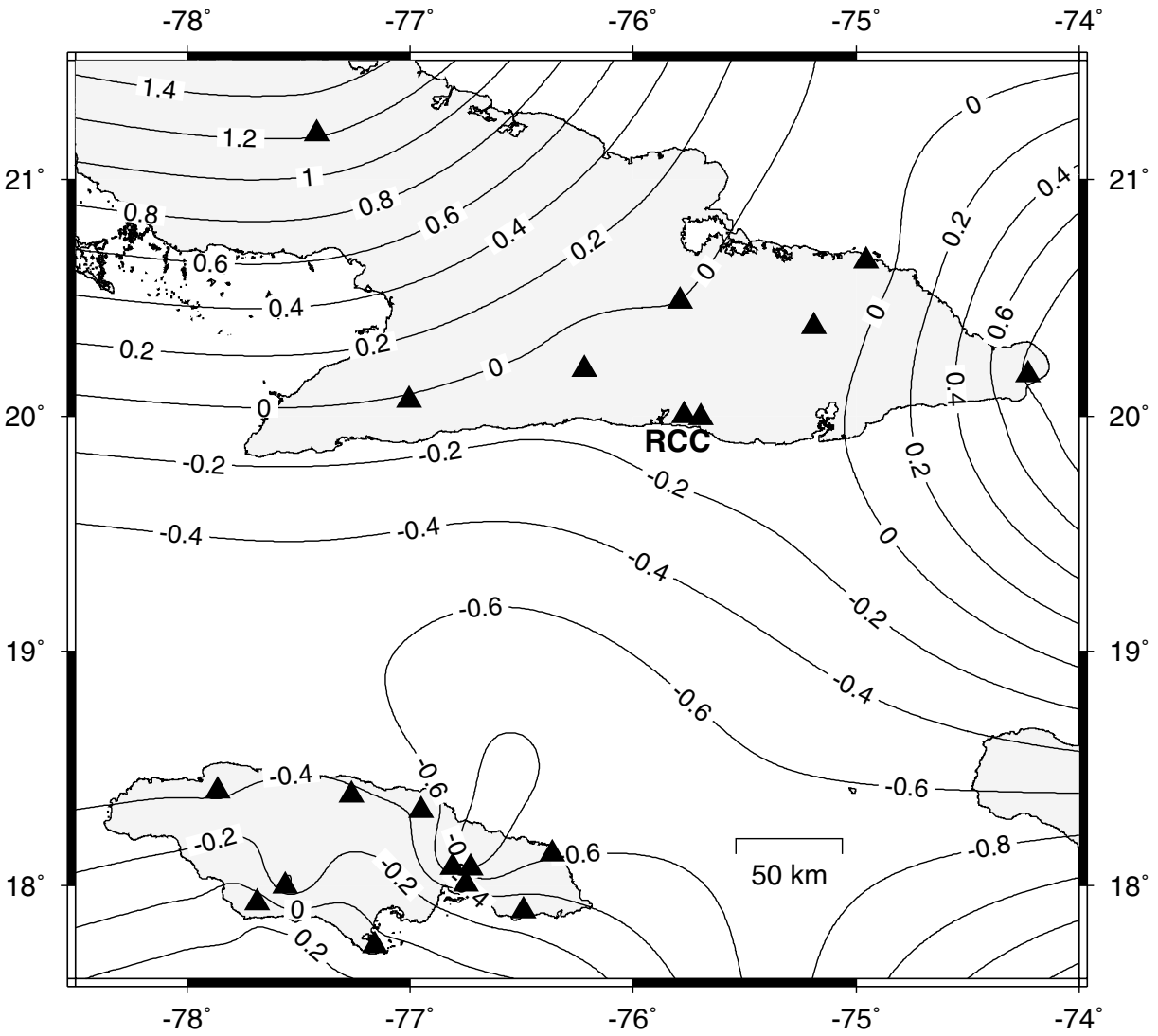

Figure 4. Contour lines showing delay times of *P* waves for each station (station corrections). The station corrections were calculated with respect to the reference station (RCC).

Snoke *et al.* (1984). The fault-plane solutions presented have nodal planes that have been resolved to within ±15°. Although each solution was constrained by seven or more polarities of the *P* wave, we categorize each solution with a quality factor based on the distribution of polarities in all quadrants and the focal-depth error. Combining these two criteria we obtain nine possible quality factors (Table 6).

4.1.1 The Cabo Cruz Basin

The CCB is a narrow E–W-trending depression, bordered on the north and south by two segments of the Oriente Fault and divided by normal faults into a series of oblique horsts and grabens (Calais & Mercier de Lépinay 1991). The discontinuous trace of the Oriente fault with left-stepping offsets generates local tensional strain and causes pull-apart subsidence (Cotilla 1993; Perrot *et al.* 1997). According to the new merged Cuba–Jamaica catalogue, the seismicity in the CCB is shallow. Note that the set of epicentres defines very well the western part of the basin (Fig. 1). We performed depth cross-sections of the hypocentres located in this zone, but no clear trend was found.

The observed focal mechanisms are consistent with E–W extension in this area (Table 7). Most fault planes are trending N55°–58°E and dipping 38°–45° to the north, which are in good agreement with the normal faults mapped by Calais & Mercier de Lépinay (1991). Small earthquakes occurring in the CCB are generated by normal faults. However, strong earthquakes should be expected along the northern and southern borders of the CCB where the major OFZ segments are located. This was the case with the last strong earthquake that occurred in this area (Perrot *et al.* 1997). The earthquake is labelled as P1 in Fig. 7 and is detailed in Table 7. The rose diagram in Fig. 7 represents the orientation of the maximum horizontal compressive stress (σ_h) obtained from the *P*, *B* and *T* axes according to Zoback (1992). Earthquakes with an unknown (U) stress regime (Tables 7 and 8) are not represented in the rose diagram. The diagram shows clear N15°E horizontal compression, in agreement with the expected W–E horizontal extension in this pull-apart zone. The lower inset in Fig. 7 shows the result of the stress inversion but this is discussed in Section 4.2.

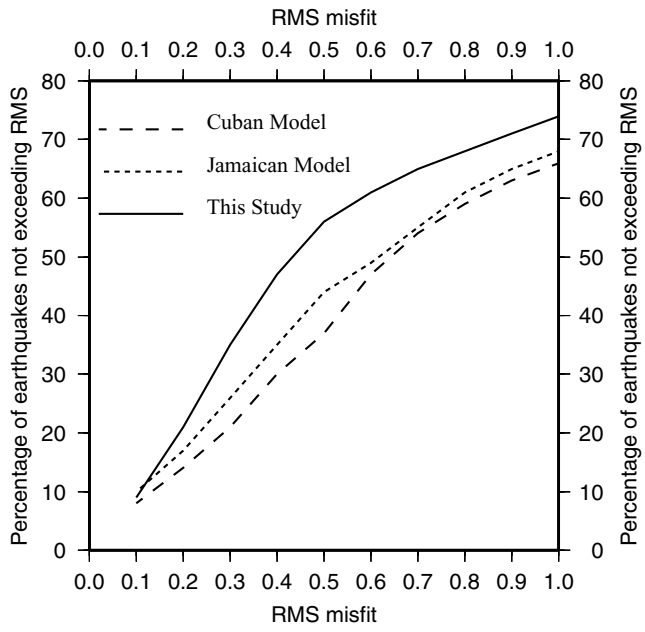

Figure 5. Percentage of the cumulative number of earthquakes having rms misfit lower than the upper limit values defining the *x*-axis. The earthquake locations (569 earthquakes) were calculated using three different models. The new velocity model shows 56 per cent of the earthquakes with an rms misfit of less than 0.5.

4.1.2 The Santiago deformed belt

The SDB was described for the first time by Calais & Mercier de Lépinay (1990, 1991). It is a narrow submarine mountain range extending over 300 km along the OFZ with folds and thrust faults showing clear evidence of transpressional deformation (Calais & Mercier de Lépinay 1990, 1991; Calais *et al.* 1998). The dashed line in Fig. 6 crossing zone 'c' represents the line of a depth cross-section (inset to Fig. 6) of earthquakes with an error in depth of less than 15 km. The depth section shows shallow and relatively deeper seismicity (deeper than 30 km). Shallow seismicity in the first 30 km measured from the north is associated with inland faults and the northern segment of the OFZ. Beyond 30 km the earthquakes are generated by thrust faults in the SDB. Deep seismicity, on the other hand, seems to be generated by reverse faults. Earthquake focal mechanisms (Fig. 8 and Table 8) in this zone show evidence of reverse faulting at depths below 30 km. It is unlikely that shallow thrust faults in SDB can be responsible for earthquakes at such depths in an oceanic crust. Another process, perhaps crustal thickening might be occurring there (see the discussion).

The focal mechanisms shown in Fig. 8 are not restricted only to the SDB; we include the segment of the OFZ (that we define as OFS), which connects the northern border of the CCB and continues eastwards along the southern Cuban margin. The events labelled as C1, C2, C3 and C4 are taken from the Harvard CMT Catalogue. Two groups of fault regimes are dominant in the area: (1) left-lateral strike-slip and (2) reverse faulting. The first group corresponds to the transition area from CCB to SDB occurring along the OFZ. The fault planes follow the trend of the OFZ and dip at 65°–80° to the north. The earthquakes located in the vicinity of the CCB (3, 13–15) have a minor normal component. However, once we move eastward the earthquakes (1, 2, 4, 5) begin to exhibit a minor reverse component. This pattern shows evidence of the transition from transtension to transpression along the OFZ. Note that the earthquakes labelled as 1, 2, 4 and 5 are not located on the mapped segment of the OFZ. The possibility that they are shifted north is low owing to the small errors in their locations. Since the resolution of seismic reflection, gravimetric and magnetic measurement throughout the area was not high enough to map the entire OFZ trace, one of the segments bordering the north side of the SDB might continue to the west. If so, then earthquakes 1, 2, 4 and 5 could be associated with one of the OFZ fault segments. The rose diagram on the upper left-hand corner plots maximum horizontal compressive stress for the events labelled as 1–5 and 13–15. It shows a clear N45°E maximum horizontal compressive stress orientation. The second group corresponds to earthquakes located in the SDB and the surrounding area, which are mainly the result of reverse faulting with variable fault plane orientations. Solutions 9 and 16 might be associated with cross-cutting compressional faults trending N100°E and caused by a discontinuity of the major Oriente transcurrent fault. In this area the trace of the Oriente fault was assumed to be caused by inadequate geophysical information and, therefore it was mapped as a dashed line. Furthermore, the assumed cross-cutting segment indicating the discontinuity might be located more to the west of where it was mapped. Note that the deformation in the coastal Cuban margins surrounding this area supports this assumption. Earthquakes with relatively deeper hypocentres such as 0 and 7 (Table 8) are unlikely to be associated with the mapped shallow thrust faults of SDB. They must be the result of another process (see the discussion). The rose diagram on the lower right-hand corner plots maximum horizontal compressive stress for the events, which belong to this group (0, 6–12, 16–20 and C1–C4). It exhibits a scattered σ_h orientation with a small tendency to be oriented in a N65°E direction. The scatter σ_h orientations might be associated with the irregular alignment of the thrust faults mapped in SDB.

4.2 Stress inversion of earthquake focal mechanisms

It has been suggested that most of the stress accumulated by the Caribbean–North American plate motion is released seismically along the northern Cuban margin during a relatively few but strong earthquakes (Perrot *et al.* 1997; Van Dusen & Doser 2000). This sparse occurrence of strong and moderate earthquakes makes it difficult to use earthquake focal mechanisms for mapping the crustal stress field in this area. The focal mechanism solutions presented in this study offer a good opportunity to estimate the principal stress orientations in this part of the Caribbean–North American plate boundary. For this purpose, we use the FMSI (Focal Mechanism Stress Inversion) software (Gephart 1990) based on procedures described in Gephart & Forsyth (1984). The modelled stress tensors and the corresponding misfit values are determined through a grid search and the misfit for a given mechanism is defined as the minimum rotation about any arbitrary axis that brings each nodal plane into compliance with the stress model being tested. The data set used in the inversion was weighted from 1 (worst) to 4 (best). We assigned weight 4 to the earthquakes labelled as P1 and C1–C4. The rest of the earthquakes were weighted from 1 to 3 according to the quality factor described in Table 6. We performed the inversion for each zone and the entire region calculating the misfit value at 5° intervals for a total of over 150 000 input models.

The results of the stress inversion for each zone are shown as the lower inset in Figs 7 and 8. Given the fact that a set of identical or nearly identical focal mechanisms cannot constrain the stress tensor (Hardebeck & Hauksson 2001), the principal stress axes for the CCB and OFS may not be well constrained by the inversion process and therefore should not be used in our interpretation. The

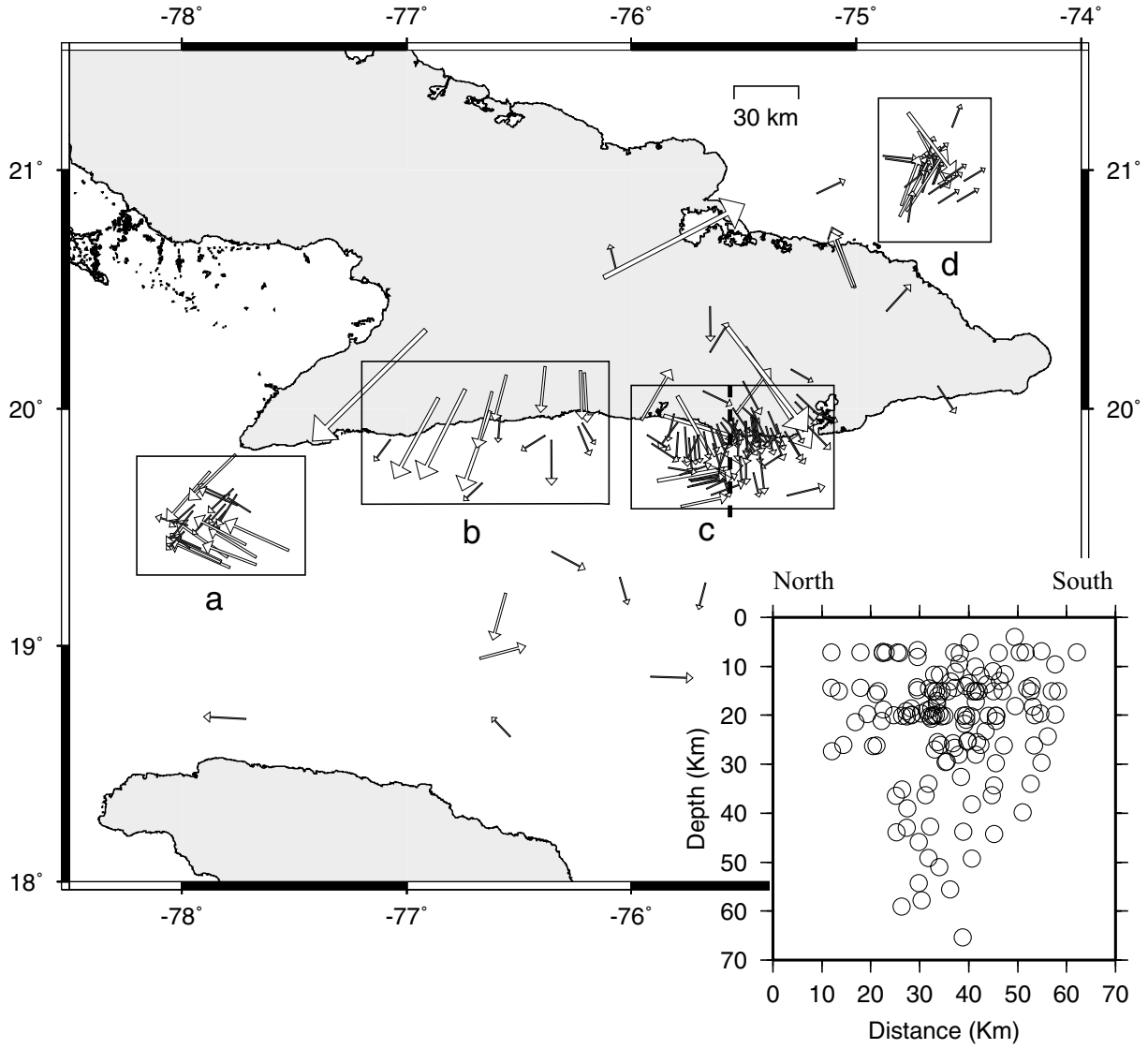

Figure 6. Epicentral changes with differences larger than 10 km between the original and the new locations. The arrows point from the original to the new locations, calculated with the velocity model obtained in this study. The original locations were computed with the Cuban velocity model without station corrections. Boxes indicate zones with distinct clustering towards significant structural features; (a) Cabo Cruz basin; (b) segments of the OFZ; (c) Santiago deformed belt; (d) junction of the NCFS and CNF. The dashed line crossing zone c represents the location of a depth cross-section (see inset) across the Santiago deformed Belt. The plotted points in the depth cross-section correspond to earthquakes having errors in depth less than 15 km.

SDB, on the other hand, shows a dissimilar focal mechanism and gives a more reliable estimation of the stress tensor. The solution shows a horizontal σ_1 (oriented ENE–WSW) with nearly vertical σ_3, indicating a thrust faulting regime.

Table 5. Number of earthquakes with error in location less than 10 km for the entire dataset (569 earthquakes) using different velocity models.

Error less than 10 km	Cuban model	Jamaica model	This study
Epicentre error radius	130	151	187
Hypocentre error radius	72	73	82
Latitude error	177	188	223
Longitude error	241	240	285
Depth error	112	111	112

Hardebeck & Hauksson (2001) proposed that a given focal mechanism data set is adequately diverse for use in stress inversions if the rms difference from the average mechanism is greater than 40°–45°. Furthermore, we have inverted only those focal mechanisms satisfying the required criteria for estimating the stress field of the entire region. In this sense, we used 28 focal mechanisms from all three data sets having sufficient levels of diversity. The resulting σ_1 is nearly horizontal in an ENE–WSW direction with near vertical σ_3, which corresponds to a thrust faulting regime (Fig. 9). This result seems to indicate that the plate boundary along the OFZ enters into a thrust faulting regime within the SDB, showing that this area is undergoing active transpressional deformation along a major transcurrent fault. This pattern is probably a result of a regional oblique motion along the OFZ (Calais & Mercier de Lépinay 1990, 1991). The orientation of the principal stress axes seems to be induced by an oblique WSW–ENE convergence of

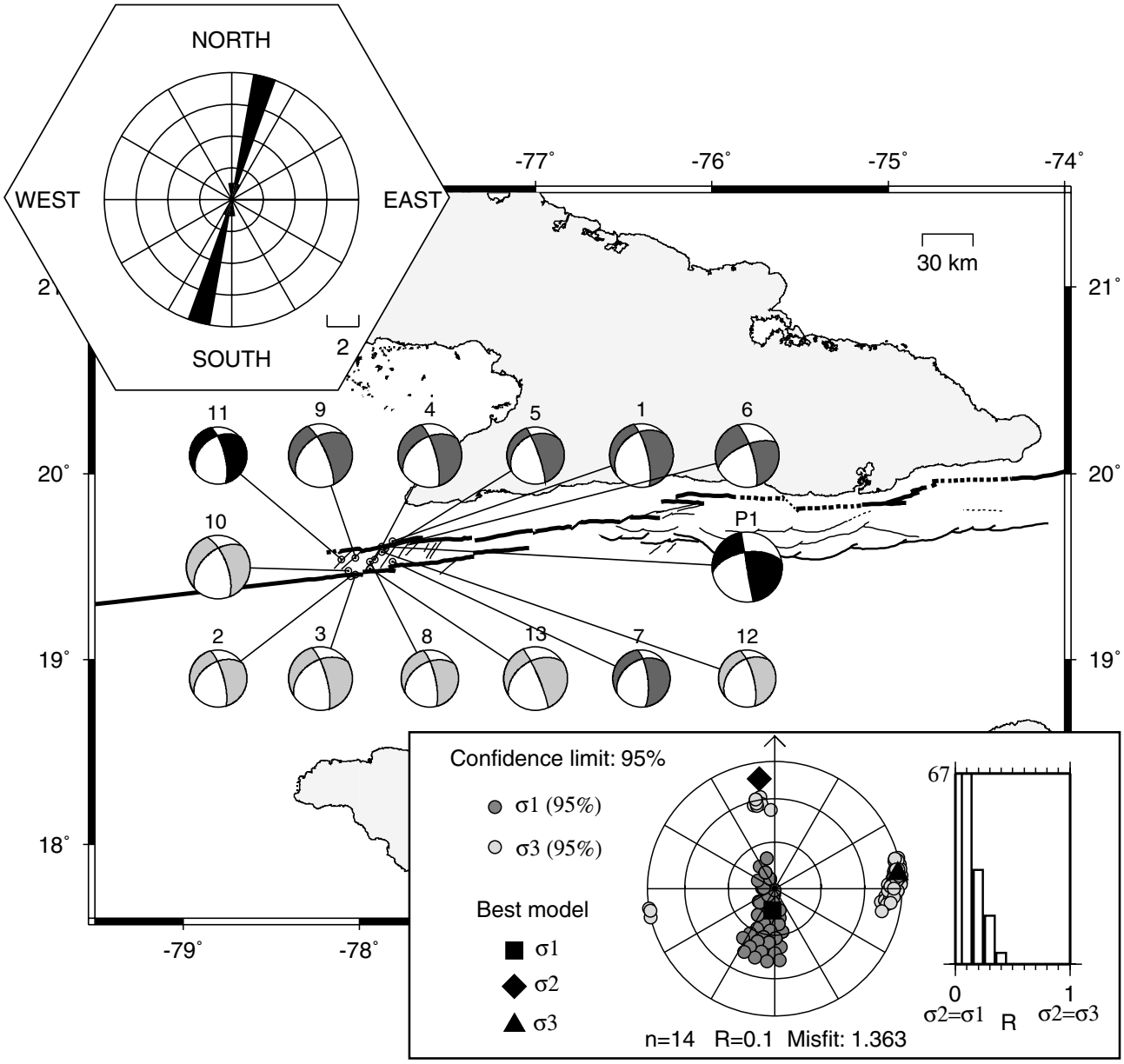

Figure 7. Earthquake focal mechanisms in the Cabo Cruz basin. The rose diagram in the upper left-hand corner shows the orientation of the maximum horizontal compressive stress (σ_h). The σ_h orientations were computed according to Zoback (1992). The earthquake labelled as P1 is from Perrot *et al.* (1997). The compressional quadrants are shaded according to the first quality index (Table 6), darkest = best and lightest = worst. The circles are sized according to the second quality index (Table 6), biggest = best and smallest = worst. The lower inset shows the result of the stress inversion (Gephart 1990) for σ_1 and σ_3 at a 95 per cent confidence level and the best model fitting the observation. The histogram shows the distribution of R defined by $R = (\sigma_2 - \sigma_1)/(\sigma_3 - \sigma_1)$ for all the models fitting the observation within a 95 per cent confidence limit.

the GM with the NAP. A summary of the stress inversion results for the three individual zones and the entire region is shown in Table 9.

5 DISCUSSION

The process of microplate formation described by several authors in previous studies seems to explain the present-day tectonic regime in this area. Oblique plate motions along strike-slip faults, rather than orthogonal plate convergence, may play an important role in the possible formation of microplates (Karig *et al.* 1986; Mann *et al.* 1995). In the case of the Gonave Microplate (GM), the development of the transpressive structure of the SDB is associated with a regional oblique relative motion of two blocks involved in strike-slip movements (Calais & Mercier de Lépinay 1991). Mullins *et al.* (1992) suggested that the northeastern corner of the Caribbean Plate (an area of the present-day Gonave Microplate) became impeded in a strike-slip restraining bend setting adjacent to the southeast extension of the Bahama carbonate platform. The GM is essentially being 'left behind' and being accreted to the North American Plate (NAP) as its eastward progress is impeded by the Bahama Platform (Mullins *et al.* 1992; Dolan & Wald 1994; Mann *et al.* 1995).

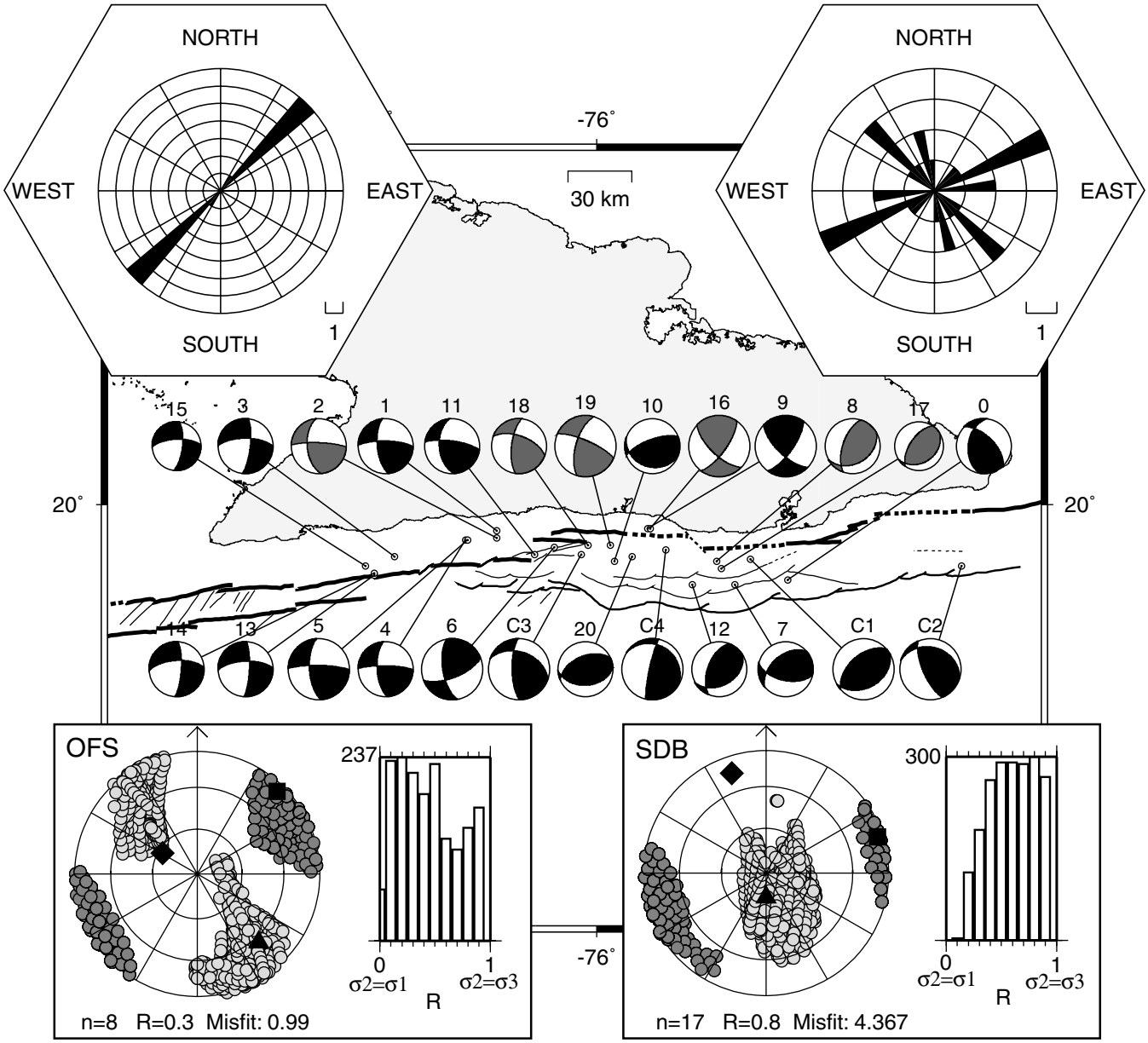

Figure 8. Earthquake focal mechanisms along the eastern part of the OFZ. Rose diagrams show the orientation of the maximum horizontal compressive stress (σ_h). The Rose diagram in the upper left-hand corner corresponds to the earthquakes 1–5 and 13–15 (OFS). The Rose diagram in the upper right-hand corner corresponds to the earthquakes 0, 6–12, 16–20 and C1–C4 (SDB). Earthquakes labelled as C1–C4 are from Harvard CMT catalogue. The lower insets show the result of the stress inversion for the two groups with symbols as in Fig. 7.

The characterization of seismicity at depth is the bottleneck for different seismotectonic interpretations in this area. Seismic reflection studies have been unable to map structures deeper than 12 km. In previous studies, Goreau (1983) noticed a high negative gravity anomaly under the deformed sediments of the Oriente Deep (the west part of SDB) and proposed the existence of a major north-dipping thrust along the southern Cuban margin. However, this structural interpretation, based on only six profiles, relies mainly on extrapolation as pointed out by Calais & Mercier de Lépinay (1991). Recent GPS measurements (De Mets *et al.* 2000) have estimated 3 ± 3 mm yr^{-1} of boundary normal convergence south of eastern Cuba, which suggest a small oblique motion (WSW–ENE) of the GM with respect to the NAP. The apparent north-dipping trend in the depth cross-section in the SDB (inset in Fig. 6) is weakly supported, taking into account the errors in depth (<15 km) of the plotted earthquakes. Bearing in mind this error, the deepest earthquakes shown in the depth cross-section may be as shallow as 30–35 km. However, previous studies (Ewing *et al.* 1960; Case *et al.*

Table 6. Quality factor definition for earthquake focal mechanisms determined from first-motion polarities. The combination of any two quality indices result in nine possible quality factors.

First quality index	Polarities distribution (strike-slip case)	Second quality index	Error in depth (less than)
A	Four quadrants	a	5 km
B	Three quadrants	b	10 km
C	Two quadrants	c	15 km

Table 7. Earthquake focal mechanism solutions for the Cabo Cruz Basin. *P*-trn, *P*-plg, *T*-trn and *T*-plg are the trend and the plunge of the *P* (compression) and *T* (tension) axes, respectively. σ_h (maximum horizontal compressive stress) directions and Reg. (faulting regime) according to Zoback (1992). *Q* (quality factor), explained in Table 6.

No	Date	Time	Lat. (N)	Lon. (W)	Dep.	Mag. (Ml)	*P* trn	*P* plg	*T* trn	*T* plg	σ_h	Reg.	Q.
1	20/05/98	1531	19.64	77.81	19	3.6	223	52	98	24	354	NF	Bb
2	29/05/98	2050	19.45	78.05	13	3.4	213	44	104	19	194	NS	Cc
3	31/05/98	0908	19.46	78.02	11	3.5	213	44	104	19	194	NS	Cb
4	02/06/98	1034	19.54	77.91	13	3.4	213	44	104	19	194	NS	Bb
5	26/06/98	1326	19.59	77.86	14	3.4	220	45	95	30	–	U	Bc
6	30/06/98	0756	19.60	77.85	15	2.9	207	29	113	8	203	SS	Bb
7	17/08/98	1748	19.53	77.81	12	3.4	224	51	107	20	197	NS	Bc
8	02/09/98	0718	19.53	77.94	26	3.2	216	44	107	19	197	NS	Cc
9	23/11/98	0523	19.55	78.02	10	3.0	205	44	96	19	186	NS	Bb
10	24/11/98	0943	19.48	78.06	26	3.4	203	48	100	11	190	NS	Cb
11	27/11/98	0131	19.54	78.10	18	3.4	217	51	100	20	190	NS	Ac
12	13/01/99	1550	19.58	77.87	26	3.3	217	51	100	20	190	NS	Cc
13	14/05/99	0529	19.49	77.94	9	3.4	209	37	99	24	–	U	Cb
P1	25/05/92	1655	19.61	77.87	19	6.9M_s	221	23	120	25	–	U	A

Table 8. Earthquake focal mechanism solutions for the eastern part of the OFZ and Santiago deformed belt. *P*-trn, *P*-plg, *T*-trn and *T*-plg are the trend and the plunge of the *P* (compression) and *T* (tension) axes, respectively. σ_h (maximum horizontal compressive stress) directions and Reg. (faulting regime) according to Zoback (1992). *Q* (quality factor), explained in Table 6.

No	Date	Time	Lat. (N)	Lon. (W)	Dep.	Mag. (Ml)	*P* trn	*P* plg	*T* trn	*T* plg	σ_h	Reg.	*Q*.
0	25/04/98	1751	19.68	75.14	34	3.2	67	9	173	59	67	TF	Ab
1	17/05/98	1954	19.89	76.45	15	3.9	41	6	134	28	41	SS	Ab
2	17/05/98	2033	19.86	76.45	15	3.3	39	16	139	31	39	SS	Bb
3	18/06/98	1454	19.78	76.91	13	2.7	230	27	137	6	227	SS	Ab
4	23/07/98	2217	19.85	76.59	16	3.3	42	10	136	25	42	SS	Ab
5	23/07/98	2319	19.85	76.58	17	3.2	42	10	136	25	42	SS	Aa
6	08/09/98	1837	19.82	76.19	18	3.3	120	2	29	35	120	SS	Aa
7	01/11/98	0408	19.66	75.38	44	3.0	167	4	70	60	167	TF	Ab
8	05/01/99	0146	19.76	75.46	32	3.2	305	14	68	65	305	TF	Bb
9	19/01/99	1503	19.90	75.77	32	3.4	86	2	354	30	86	SS	Aa
10	04/02/99	0933	19.76	75.92	17	3.2	352	24	136	61	352	TF	Ab
11	05/02/99	0246	19.79	76.28	20	3.1	42	15	144	38	42	SS	Ab
12	13/02/99	2042	19.66	75.57	30	3.2	308	9	62	68	308	TF	Ab
13	29/03/99	0859	19.70	77.00	8	3.3	227	25	133	8	223	SS	Ab
14	29/03/99	1135	19.71	77.00	12	3.4	227	29	133	7	223	SS	Ab
15	20/04/99	0031	19.74	77.04	9	3.4	228	31	137	1	227	SS	Ac
16	28/05/99	1136	19.90	75.76	32	3.4	86	2	354	30	86	SS	Ba
17	15/06/99	0730	19.73	75.44	21	3.4	313	15	97	72	313	TF	Bc
18	22/09/99	1933	19.83	76.04	26	3.3	240	5	146	38	240	SS	Bb
19	26/09/99	1338	19.83	75.94	26	3.4	63	7	157	29	63	SS	Ba
20	16/12/99	0322	19.78	75.84	16	4.4	346	5	102	79	346	TF	Ab
C1	01/09/85	0101	19.77	75.31	10	5.0Mw	324	7	104	80	324	TF	?
C2	12/02/89	1426	19.74	74.36	25	5.2Mw	230	23	97	58	230	TF	?
C3	05/22/90	2035	19.79	76.07	15	5.3Mw	241	17	131	47	241	TS	?
C4	09/04/90	0803	19.81	75.69	15	5.2Mw	265	35	123	49	–	U	?

1990) have estimated a Moho depth of 10–21 km in this area. Therefore, the observed deep seismicity suggests that there may be a significant increase in the crustal thickness around the SDB. The focal mechanism of the deepest earthquake in Fig. 8 (event number 7), with a depth of 44 km (Table 8), shows reverse faulting with a small strike-slip component, which may support an underthrusting of the GM beneath the Cuban block in the SDB area as was suggested by Enman *et al.* (1997).

Another important feature is the earthquake activity in the interior part of the GM (Fig. 1). Geophysical investigations of the Caribbean crust have revealed several scarps, mostly NE–SW-oriented, on the seafloor in the interior part of the GM (Donnelly 1994), which suggest that the GM is undergoing internal deformation. Continued movement along both the northern and southern strike-slip boundaries of the GM has resulted in internal deformation of the microplate (Mann *et al.* 1995), with NE–SW-oriented structures probably being reactivated in normal faulting.

6 CONCLUSIONS

The combined Cuban and Jamaican catalogues over a period of 2 years allowed us to obtain for the first time a 1-D *P*-wave velocity model based on local seismic data. The model represents a significant improvement in the earthquake locations and can be used as an initial reference model for seismic tomography.

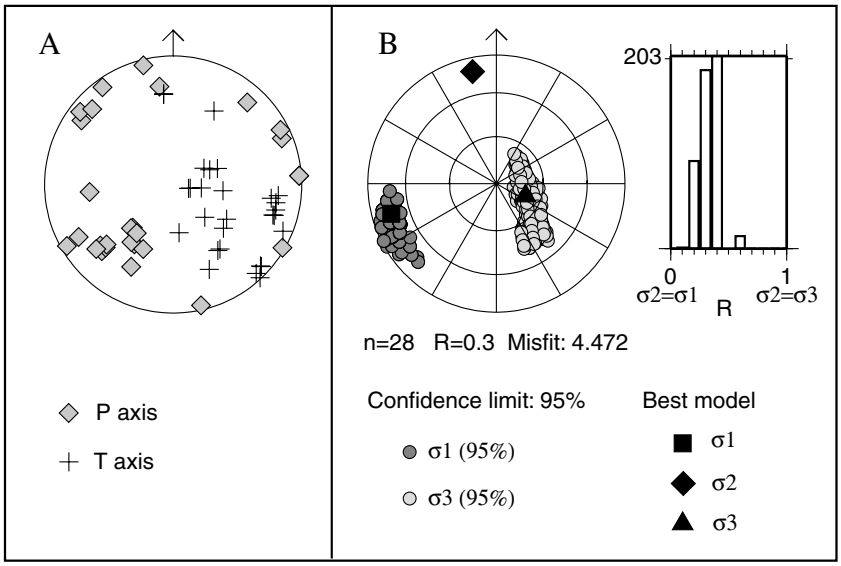

Figure 9. Stress inversion result for the entire region. (a) The *P* and *T* axes of the focal mechanisms used in the inversion. (b) The obtained principal stress axes within a 95 per cent confidence limit and the best model fitting the observation.

Table 9. Earthquake focal mechanism stress inversion results for the three areas and the entire region. R is defined by $R = (\sigma_2 - \sigma_1)/(\sigma_3 - \sigma_1)$.

Area	No of F.M.	FMSI misfit	R	σ_1		σ_2		σ_3	
				trn	plg	trn	plg	trn	plg
CCB	14	1.363	0.1	186	76	352	14	83	3
OFS	8	0.99	0.3	44	7	301	63	138	26
SDB	17	4.367	0.8	72	5	341	15	180	74
Entire region	28	4.472	0.3	254	16	348	12	113	70

The seismicity along the plate boundary is shallow in the west but increases in depth eastward. It is concentrated along two local structures: (1) the CCB and (2) the SDB. Deep seismicity seems to be restricted only to the SDB.

Despite the limited data set, recorded over only 2 years, the new earthquake locations permit us to identify and characterize the tectonic regime along the OFZ. The CCB is dominated by transtension and the SDB by transpression. The earthquake focal mechanisms along these structures show evidence that transtension and transpression are occurring at the same time and at short distances along a major transcurrent fault, the Oriente fault.

The stress field for the entire region is suggested to be transpressional, which is in agreement with the dominant structural trend associated with the SDB. The principal stress axes are well constrained from the inversion of focal mechanisms within a 95 per cent confidence level. They have a near horizontal σ_1 (ENE–WSW-oriented) and a nearly vertical σ_3, indicating a thrust faulting regime.

The deep seismicity in the SDB and the thrust faulting regime obtained from the stress inversion seem to support the previously suggested underthrusting of the GM beneath the Cuban block (Enman *et al.* 1997), which probably causes a crustal thickening in the SDB area.

ACKNOWLEDGMENTS

This work was supported by a grant from the government of Norway. The Jamaican and Cuban Seismic Network are funded entirely by their respective governments. We thank the staff at the Cuban Seismological Service and the staff at the Earthquake Unit, Jamaica for their hospitality and support during the data collection. The comments of Eric Calais and Diane Doser greatly improved this work

REFERENCES

Alvarez, J., Blanco, P., Medvedev, S.V., Menende, L. & Shteynberg, V.V., 1973. The seismic conditions of Santiago de Cuba, *Bull. (Izv.) Acad. Sci. USSR, Earth Phys.,* **5,** 320–324.

Arden, D.D., 1975. Geology of Jamaica and the Nicaragua Rise, in *The Ocean Basins and Margins,* Vol. 3, pp. 617–661, eds Nairn, A.E.M. & Stehli, F.G., Plenum, New York.

Bush, V.A. & Shcherbakova, I.N., 1986. New data on the deep tectonics of Cuba, *Geotectonics,* **20,** 192–203.

Calais, E. & Mercier de Lépinay, B., 1990. A natural model of active transpressional tectonics: the *en échelon* structures of the Oriente deep along the northern Caribbean transcurrent plate boundary (Southern Cuban margin), *Rev. Inst. Fr. Pét.,* **45,** 147–160.

Calais, E. & Mercier de Lépinay, B., 1991. From transtension to transpression along the Southern Caribbean plate boundary off Cuba: implications for the recent motion of the Caribbean plate, *Tectonophysics,* **186,** 329–350.

Calais, E., Perrot, J. & Mercier de Lépinay, B., 1998. Strike-slip tectonics and seismicity along the Northern Caribbean plate boundary from Cuba to Hispaniola, in *Active Strike-slip and Collisional Tectonics of the Northern Caribbean Plate Boundary Zone,* Vol. 326, pp. 125–142, eds Dolan, J.F. & Mann, P., Geol. Soc. Am. Special Paper, Boulder, CO.

Case, J.E., MacDonald, W.D. & Fox, P.J., 1990. Caribbean crustal provinces; seismic and gravity evidence, in *The Geology of North America, The Caribbean Region,* Vol. H, pp. 15–36, eds Dengo, G. & Case, J.E., Geol. Soc. Am., Boulder, CO.

Cotilla, M., 1993. A seismotectonic characterization of Cuba, *PhD thesis,* Inst. of Geophysics and Astronomy, Acad. of Sciences of Cuba, Havana, p. 200.

Cotilla, M., 1998. An overview on the seismicity of Cuba, *J. Seismol.,* **2,** 323–335.

De Mets, C., Gordon, R.G., Argus, D.F. & Stein, S., 1990. Current plate motions, *Geophys. J. R. astr. Soc.,* **101,** 425–478.

De Mets, C., Jansma, P.E., Mattioli, G.S., Dixon, T., Farina, P., Bilham, R., Calais, E. & Mann, P., 2000. GPS geodetic constraints on Caribbean–North American Plate motion, *Geophys. Res. Lett.,* **27,** 437–440.

Deng, J. & Sykes, L.R., 1995. Determination of Euler pole for contemporary relative motion of the Caribbean and North American plates using slip vectors of interplate earthquakes, *Tectonics,* **14,** 39–53.

Dixon, T.H., Farina, F., Demets, C., Jansma, P., Mann, P. & Calais, E., 1998. Relative motion between the Caribbean and North American plates and related boundary zone deformation from a decade of GPS observations, *J. geophys. Res.,* **103,** 15 157–15 182.

Donnelly, T.W., 1994. The Caribbean Sea floor, in *Caribbean Geology: an Introduction,* pp. 41–63, UWI Publishers' Association, Kingston.

Dolan, J.F. & Wald, D.J., 1994. Consequences of time-transgressive, oblique underthrusting of the southeastern Bahamas: localization of large thrust earthquakes and controls on large-scale forearc subsidence events, *Geol. Soc. Am., Abstr. Programs,* **26,** A–251.

Edgar, N.T., Ewing, J.I. & Hennion, J., 1971. Seismic refraction and reflection in the Caribbean Sea, *Am. Assoc. Petr. Geol. Bull.,* **55,** 833–870.

Enman, S.V., Belousov, T.P., Marquez, M.E., Rueda, J.S. & Jorge, G.D., 1997. Recent crustal movements and morphostructural pattern of Southeastern Cuba: Santiago de Cuba Geodynamic Research Site, *Izvest. Phys. Solid Earth,* **1,** 55–69.

Ewing, J., Antoine, J. & Ewing, M., 1960. Geophysical measurements in the western Caribbean Sea and in the Gulf of Mexico, *J. geophys. Res.,* **65,** 4087–4126.

Gephart, J.W., 1990. FMSI: a FORTRAN program for inverting fault/slickenside and earthquake focal mechanism data to obtain the regional stress tensor, *Comp. Geosci.,* **16,** 953–989.

Gephart, J.W. & Forsyth, D.W., 1984. An improved method for determining the regional stress tensor using earthquake focal mechanism data: application to the San Fernando earthquake sequence, *J. geophys. Res.,* **89,** 9305–9320.

Goreau, P.D.E., 1983. The tectonic evolution of the north-central Caribbean plate margin, *PhD thesis,* Woods Hole Oceanographic Institution, WHOI83–84, p. 245.

Hardebeck, J.L. & Hauksson, E., 2001. Crustal stress field in southern California and its implications for fault mechanics, *J. geophys. Res.,* **106,** 21 859–21 882.

Havskov, J. & Otemöller, L., 1999. SEISAN: the earthquake analysis software, Version 7.0, Institute of Solid Earth Physics, University of Bergen, Norway, p. 226.

Karig, D.E., Sarewitz, D.R. & Haeck, G.D., 1986. Role of strike-slip faulting in the evolution of allochthonous terranes in the Philippines, *Geology,* **14,** 852–855.

Kissling, E., 1988. Geotomography with local earthquake data, *Rev. Geophys.,* **26,** 659–698.

Kissling, E., Ellsworth, W.L., Eberhart Phillips, D. & Kradolfer, U., 1994. Initial reference models in local earthquake tomography, *J. geophys. Res.,* **99,** 19 635–19 646.

Kissling, E., Kradolfer, U. & Maurer, H., 1995. VELEST user's guide—short introduction, Institute of Geophysics and Swiss Seismological Service, ETH Zürich, p. 25.

Lay, T. & Wallace, T.C., 1995. *Modern Global Seismology,* pp. 80–86, Academic, New York.

Lienert, B.R. & Havskov, J., 1995. A computer program for locating earthquakes both locally and globally, *Seism. Res. Lett.,* **66,** 26–36.

Mann, P., Taylor, F.W., Lawrence Edwards, R. & Teh-Lung, Ku., 1995. Actively evolving microplate formation by oblique collision and sideways motion along strike-slip faults: an example from the northeastern Caribbean plate margin, *Tectonophysics,* **246,** 1–69.

Moreno, B., 2002. The new Cuban Seismograph Network, *Seism. Res. Lett.,* **73,** 505–518.

Mullins, H.T. *et al.*, 1992. Carbonate platforms along the southeast Bahamas–Hispaniola collision zone, *Mar. Geol.,* **105,** 169–209.

Perrot, J., Calais, E. & Mercier de Lépinay, B., 1997. Tectonic and kinematic regime along the Northern Caribbean Plate Boundary: new insights from broad-band modeling of the May 25, 1992, $M_s = 6.9$ Cabo Cruz, Cuba, earthquake, *Pure appl. Geophys.,* **147,** 475–487.

Snoke, J.A., Munsey, J.W., Teague, A.G. & Bollinger G.A., 1984. A program for focal mechanism determination by combined use of polarity and SV–P amplitude ratio data, *Earthquake Notes,* **55,** 1–15.

Sykes, L.R., McCann, W.R. & Kafka, A.L., 1982. Motion of the Caribbean plate during the last 7 million years and implications for earlier Cenozoic movements, *J. geophys. Res.,* **13,** 10 656–10 676.

Van Dusen, S. & Doser, D., 2000. Faulting processes of historic (1917–1962) $M \geq 6.0$ earthquakes along the north-central Caribbean Margin, *Pure appl. Geophys.,* **157,** 719–736.

Wiggins-Grandison, M., 2001. Preliminary results from the new Jamaican seismograph network, *Seism. Res. Lett.,* **72,** 525–537.

Zoback, M.L., 1992. First and second-order lithospheric stress patterns, *J. geophys. Res.,* **97,** 11 703–11 728.